molecules

MDPI

Article

Scaling of Rotational Constants

Denis S. Tikhonov [1,*,†,‡], Colin J. Sueyoshi [2,§], Wenhao Sun [1], Fan Xie [1], Maria Khon [1,3], Eva Gougoula [1], Jiayi Li [1,3], Freya Berggötz [1,4], Himanshi Singh [1,3], Christina M. Tonauer [1] and Melanie Schnell [1,3,*]

1 Deutsches Elektronen-Synchrotron DESY, Notkestr. 85 , 22607 Hamburg, Germany
2 Department of Chemistry, Amherst College, Amherst, MA 01002-5000, USA
3 Institute of Physical Chemistry, Christian-Albrechts-Universität zu Kiel, 24118 Kiel, Germany
4 Department of Physics, Universität Hamburg, 22607 Hamburg, Germany
* Correspondence: denis.tikhonov@desy.de (D.S.T.); melanie.schnell@desy.de (M.S.)
† Current address: Center for Free-Electron Laser Science CFEL, Deutsches Elektronen-Synchrotron DESY, Notkestr. 85, 22607 Hamburg, Germany.
‡ Free Moscow University; https://freemoscow.university/.
§ Work was done during an internship at Deutsches Elektronen-Synchrotron DESY.

Abstract: This manuscript introduces the concept of scaling factors for rotational constants. These factors are designed to bring computed equilibrium rotational constants closer to experimentally fitted ground-state-averaged rotational constants. The parameterization of the scaling factors was performed for several levels of theory, namely DF-Dn/def2-mVP (DF = B3LYP, PBE0, n = 3(BJ), 4, m = S, TZ), PBEh-3c, and r^{2}SCAN-3c. The obtained scaling factors systematically improved the consistency between the theoretical and experimental rotational constants.

Keywords: rotational constants; scaling factors; density functional theory

Citation: Tikhonov, D.S.; Sueyoshi, C.J.; Sun, W.; Xie, F.; Khon, M.; Gougoula, E.; Li, J.; Berggötz, F.; Singh, H.; Tonauer, C.M.; Schnell, M. Scaling of Rotational Constants. *Molecules* **2024**, *29*, 5874. https://doi.org/10.3390/molecules29245874

Academic Editors: Rui Fausto and Gulce Ogruc Ildiz

Received: 7 November 2024
Revised: 2 December 2024
Accepted: 4 December 2024
Published: 12 December 2024

1. Introduction

Rotational spectroscopy, consisting of microwave (MW) [1,2], millimeter wave (MMW) [3], and terahertz (THz) [4–6] spectroscopies, is a powerful high-resolution experimental technique that provides unprecedented structural sensitivity for the different structural (including conformational) and constitutional isomerisms of molecules [7–9], as well as for isotopic substitutions and various large-amplitude vibrational motions [10], such as proton transfer [11], internal rotation [12], inversion [13], and even movements of an entire molecule across another molecule's surface [9]. This kind of spectroscopic technique can be used in various applications, from monitoring the chemical composition of mixtures [14] and reactions [3,15] to detecting atmospheric [16,17] and interstellar molecular species [8,18].

In the zeroth approximation, the rotational spectrum of a molecule is given by the rigid rotor model, which in the case of non-linear molecules is parametrized using three rotational constants, which are denoted as A, B, and C or, equivalently, as B_a, B_b, and B_c, respectively [19–21]. These constants, usually expressed in MHz, are related to the moments of inertia I_α along the given α-th principal axis of the molecule through the following expression [19,20]:

$$B_\alpha = \frac{\hbar}{4\pi I_\alpha}\,, \tag{1}$$

where $\alpha = a, b, c$ is the given principal axis, $\hbar = 1.05 \times 10^{-34}$ J·s is the reduced Planck constant, and the moment of inertia is given as

$$I_\alpha = \sum_{n=1}^{N} m_n \cdot r_{\alpha n}^2\,, \tag{2}$$

where n enumerates the atoms in the molecule, N is the overall number of atoms in the molecule, m_n is the mass of the n-th atom, and $r_{\alpha n}$ is the distance of the n-th atom to the α-th

principal axis. In the experiment, the so-called vibrationally averaged rotational constants are obtained, usually in the ground vibrational state, and they are commonly denoted as A_0, B_0, and C_0 [21].

The initial structural assignment of a spectroscopically observed species is usually conducted based on quantum–chemical (QC) calculations. The candidate structures are optimized at a chosen level of theory, usually with a dispersion-corrected density functional theory (DFT) calculation, and then the theoretical rotational constants are compared with the experimentally determined ones [22]. However, such a comparison does not always yield an unambiguous assignment of the molecular structures, and the reason for this is two-fold. First of all, the optimized structure corresponds to the so-called equilibrium geometry with the corresponding equilibrium rotational constants A_e, B_e, and C_e, in which all vibrational effects are absent [21,23]. Therefore, the experimental A_0, B_0, and C_0 values and theoretical A_e, B_e, and C_e are not equal due to the vibrational anharmonic shifts, which usually expand the molecular size, thus increasing the moments of inertia (Equation (2)) and consequently decreasing the corresponding rotational constant (Equation (1)) [24]. In other words, it is generally expected that $B_{0,\alpha} \leq B_{e,\alpha}$. The second reason is the quality of the QC approximation, which can distort the equilibrium structure due to the complicated underestimation and/or overestimation of various intra- and intermolecular chemical bonds and non-covalent interactions. This systematic error does not have a preferred shift of the rotational constant values with respect to their experimental counterparts and thus can be of any type [21].

In this work, we propose to systematically improve the inconsistency between experimental ground-state-averaged rotational constants (A_0, B_0, C_0) and their theoretical equilibrium counterparts (A_e, B_e, C_e) by applying tabulated scaling factors. Such an approach, where the band shifts due to anharmonic effects and QC approximation failure, has been demonstrated to be fruitful in the case of vibrational (e.g., infrared) spectroscopy [25–32]. Therefore, it is interesting to investigate whether a similar systematic improvement for the lower-frequency spectral range can be achieved as well. First, we will introduce the procedure of the scaling, the fitting model, and the training dataset; then, we will provide the scaling factors, and in the end, we will give an application example using a few recently studied systems with the usage of the PBE0-D3(BJ)/def2-TZVP level of theory.

2. Scaling Procedure

We propose to perform the scaling of the theoretical equilibrium constants obtained from QC calculations (A_e^{QC}, B_e^{QC}, C_e^{QC}) with a single global scaling factor, s, for a given QC approximation, such that the adjusted constants A_s, B_s, and C_s are defined as

$$\begin{cases} A_s = s \cdot A_e^{QC}, \\ B_s = s \cdot B_e^{QC}, \\ C_s = s \cdot C_e^{QC}. \end{cases} \quad (3)$$

Since the rotational constants are inversely proportional to the moments of inertia (see Equations (1) and (2)), such a scaling procedure is effectively equivalent to the global scaling of the atomic coordinates:

$$\mathbf{r}_{s,n} = \frac{\mathbf{r}_{e,n}}{\sqrt{s}}, \quad (4)$$

where $\mathbf{r}_{e,n}$ and $\mathbf{r}_{s,n}$ are the equilibrium and scaled positions of the n-th atom in the molecule (see Equation (2)).

The scale factors are supposed to work as follows. The user optimizes the molecular geometry at a given level of theory to produce the equilibrium rotational constants (A_e^{QC}, B_e^{QC}, C_e^{QC}). Then, a single tabulated scale factor, s, is taken. These rotational constants are multiplied with this factor, as given in Equation (3), to produce scaled rotational constants (A_s, B_s, C_s), which by design should better resemble the experimentally measured values.

Then, the comparison of the experimental and scaled rotational constants can be made, e.g., to identify particular conformers in the gas phase (see refs. [7,9,15,22,33]).

To determine and tabulate the scaling factors s for given QC approximations, we need a benchmark dataset. In this case, we chose the set of molecules used for obtaining the scaling factors for harmonic frequencies from ref. [34], which were computed using ORCA 5 software [35,36]. From the set of 441 neutral singlet molecules, 174 non-linear molecules with up to 17 atoms with experimentally available A_0, B_0, and C_0 values were selected. Only the relatively high-quality QC approximations were considered here, namely DF-Dn/def2-mVP (DF = B3LYP, PBE0; n = 3(BJ), 4; m = S, TZ) [37–43], PBEh-3c [44], and r^{2}SCAN-3c [45] levels of theory, while the calculations with the 6-31G basis set were left out from the discussion here. This was performed since rotational spectroscopy, as a high-resolution technique, generally requires more high-quality data for comparison than rotationally unresolved infrared spectroscopy. In addition, MW spectroscopy, as the lowest frequency gas-phase spectroscopic technique to this date, is practically limited by the size of the systems that can be brought into the gas phase in sufficient amounts and by the spectral resolution, as for large systems, the spectra will become dense and uninterpretable, despite the experimental resolution being of the order of $\Delta\nu/\nu \sim 10^{-6}$–$10^{-7}$ in the standard arrangement [46].

As the values of the rotational constants $A \geq B \geq C$ can differ by orders of magnitude, the metrics that use the absolute deviations between the experimental and theoretical rotational constants are essentially useless, as they will mostly fit the A-rotational constants for small-size molecules. Therefore, an advantageous approach is switching to relative values fitting, which was introduced in ref. [34]. In its application to rotational constants, the least-squares problem can be written in the following way:

$$\mathrm{rRSMD}^2(s) = \\ = \sum_{k=1}^{N_\mathrm{mol}} \left(\left(s \cdot \frac{A_{\mathrm{e},k}^\mathrm{QC}}{A_{0,k}^\mathrm{exp}} - 1 \right)^2 + \left(s \cdot \frac{B_{\mathrm{e},k}^\mathrm{QC}}{B_{0,k}^\mathrm{exp}} - 1 \right)^2 + \left(s \cdot \frac{C_{\mathrm{e},k}^\mathrm{QC}}{C_{0,k}^\mathrm{exp}} - 1 \right)^2 \right) \to \min\,, \quad (5)$$

where rRMSD denotes the relative root mean square deviation (rRMSD) of the rotational constants, k enumerates the molecules in the dataset, and N_mol is the total number of molecules in the dataset. The optimal scaling factors are thus given via the following equation [34]:

$$s_\mathrm{opt} = \underset{s}{\mathrm{argmin}} \left(\mathrm{rRSMD}^2(s) \right) = \frac{\sum_{k=1}^{N_\mathrm{mol}} \left(\frac{A_{\mathrm{e},k}^\mathrm{QC}}{A_{0,k}^\mathrm{exp}} + \frac{B_{\mathrm{e},k}^\mathrm{QC}}{B_{0,k}^\mathrm{exp}} + \frac{C_{\mathrm{e},k}^\mathrm{QC}}{C_{0,k}^\mathrm{exp}} \right)}{\sum_{k=1}^{N_\mathrm{mol}} \left(\left(\frac{A_{\mathrm{e},k}^\mathrm{QC}}{A_{0,k}^\mathrm{exp}} \right)^2 + \left(\frac{B_{\mathrm{e},k}^\mathrm{QC}}{B_{0,k}^\mathrm{exp}} \right)^2 + \left(\frac{C_{\mathrm{e},k}^\mathrm{QC}}{C_{0,k}^\mathrm{exp}} \right)^2 \right)}\,, \quad (6)$$

where argmin denotes the minimal value of s, which minimizes the corresponding function value. The fitting uncertainty of this value is given by the following equation:

$$\sigma_\mathrm{opt} = \frac{\mathrm{rRSMD}(s_\mathrm{opt})}{\sqrt{\sum_{k=1}^{N_\mathrm{mol}} \left(\left(\frac{A_{\mathrm{e},k}^\mathrm{QC}}{A_{0,k}^\mathrm{exp}} \right)^2 + \left(\frac{B_{\mathrm{e},k}^\mathrm{QC}}{B_{0,k}^\mathrm{exp}} \right)^2 + \left(\frac{C_{\mathrm{e},k}^\mathrm{QC}}{C_{0,k}^\mathrm{exp}} \right)^2 \right)}}\,, \quad (7)$$

where $\mathrm{rRSMD}(s_\mathrm{opt})$ is the value of the rRMSD (Equation (5)), with the optimal scaling factor given in Equation (6). Note that we do not use weighting with the standard deviations of the experimental fits here because the theoretical calculations have much larger systematic uncertainties that we cannot account for.

3. Resulting Scaling Factors

The resulting scaling factors for various levels of theory, as well as the rRMSD values (Equation (5)) for the unscaled and optimally scaled theoretical rotational constants, are given in Table 1. Several trends can be observed from these results. First, the scaling improved the match between the theory and experiment in most cases, except for B3LYP-Dn/def2-TZVP (n = 3(BJ), 4), which we will discuss later. We also see that the increase in the basis set quality from def2-SVP to def2-TZVP improved the agreement between the experiment and theory in both scaled and unscaled cases. Applying either the D3(BJ) or D4 dispersion correction led to the same scaling factors, which probably points to the equal performance of these corrections. A similar trend was observed for the harmonic frequency scaling factors in ref. [34]. However, the most unexpected yet predictable result is that the optimal scaling factors for the B3LYP-Dn/def2-TZVP levels of theory were equal to one within the margins of error. This means that the scaling did not significantly improve the predicted rotational constant at this approximation. At the same time, the rRMSD values for the B3LYP-Dn/def2-TZVP levels are amongst the best in the dataset. Such behavior matches the popularity of these levels of theory for quantum–chemical computations among the rotational spectroscopy community.

Table 1. Optimal scaling factors for rotational constants (s_{opt}) and their uncertainties (σ_{opt}) were determined for the listed quantum–chemical approximations with Equations (6) and (7), respectively. rRMSD denotes the values of the relative root mean square deviation (Equation (5)) computed for the training dataset without scaling ($s = 1$) and with an optimized scaling factor ($s = s_{opt}$).

Method			$s_{opt} \pm \sigma_{opt}$	**rRMSD(s)×100%**	
DF	**Dn**	**Basis**		$s = 1$	$s = s_{opt}$
B3LYP	D3(BJ)	def2-SVP	1.008 ± 0.001	2.748	2.645
		def2-TZVP	1.000 ± 0.001	2.225	2.225
	D4	def2-SVP	1.008 ± 0.001	2.765	2.656
		def2-TZVP	1.000 ± 0.001	2.244	2.244
PBE0	D3(BJ)	def2-SVP	0.995 ± 0.001	2.633	2.579
		def2-TZVP	0.988 ± 0.001	2.530	2.202
	D4	def2-SVP	0.995 ± 0.001	2.637	2.583
		def2-TZVP	0.988 ± 0.001	2.535	2.206
	PBEh-3c		0.987 ± 0.001	3.092	2.778
	r^{2}SCAN-3c		1.008 ± 0.001	2.689	2.577

4. Illustrative Cases

The simplest way to illustrate the robustness and generality of the scaling procedure is to apply this procedure to cases outside the training dataset. For this, we demonstrate the applicability of the obtained scaling factors for a popular quantum–chemical approximation, namely PBE0-D3(BJ)/def2-TZVP [40–42]. The geometries of the molecules discussed here were optimized at this level of theory using the ORCA 5 [35,36] software, and then their rotational constants were taken from the calculations. In the case of isotopic substitutions, the rotational constants of the isotopologues were re-computed from the optimized geometries using the UNEX 1.6 software [47]. To demonstrate the numerical performance of the scaling factor, we compared the rRMSD (Equation (5)) and mean absolute deviations (MADs) of the rotational constants from the experimentally determined values for the given molecules in the case of scaled and unscaled theoretical equilibrium rotational constants. The MAD values were calculated according to the following expression:

$$\mathrm{MAD}(s) = \sum_{k=1}^{N_{mol}} \left(\left| s \cdot A_{e,k}^{QC} - A_{0,k}^{exp} \right| + \left| s \cdot B_{e,k}^{QC} - B_{0,k}^{exp} \right| + \left| s \cdot C_{e,k}^{QC} - C_{0,k}^{exp} \right| \right). \quad (8)$$

The first illustrative set of molecules included 15 linear top molecules from di- to pentatomic molecules. Since linear molecules have only one rotational constant, they were excluded from the training set, and the scaling effect on these systems will be the most clearly visible. The calculation of the rRMSD and MAD values (Equations (5) and (8)) for the linear molecules, thus, included only the B rotational constant. The second illustrative set was the case of isotopologues, which, for the simplicity of the analysis, were not included in the training dataset. We chose single-substituted isotopologues of imidazole ($C_3H_4N_2$), which had rotational constants of three singly substituted ^{13}C and two singly substituted ^{15}N isotopologues available from the literature [48]. The last example was a set of non-covalently bound molecular systems, namely, water–hydrochloric acid clusters $HCl(H_2O)_n$ $(n = 2–5, 7)$, which are examples of hydrogen bond network structures. The rotational constants for these species were taken from refs. [33,49].

We can first take a look at a few exemplary cases of molecular systems from our test dataset, including two linear molecules (HCN and HCCCN), one imidazole ^{15}N-substituted isotopologue, namely imidazole-$^{15}N(1)$ (nomenclature adapted from ref. [48]), and also the largest of our hydrochloric acid clusters, $HCl(H_2O)_7$. The structures of these molecules and their rotational constants are given in Figure 1 and Table 2. As one can see, B3LYP-D3(BJ)/def2-TZVP provided a reasonable estimation of the rotational constants, closer to the experimental values than the unscaled constants at the PBE0-D3(BJ)/def2-TZVP level of theory. However, PBE0-D3(BJ)/def2-TZVP after scaling became as accurate or even more accurate than the B3LYP-D3(BJ)/def2-TZVP-based results. This can be seen by comparing the deviations within the datasets. By looking at the rRMSD and MAD values for the scaled and unscaled rotational constants of these systems at the PBE0-D3(BJ)/def2-TZVP level of theory (Table 3), we observe that the scaling indeed improved the agreement of the theoretical and experimental values. Note that the rRMSD and MAD deviations for the non-covalently bound cluster are larger than for the covalently bound linear molecules and imidazole isotopologues. This might be either due to the less stiff nature of the intermolecular bonds, which allows for larger systematic deviations of the obtained numerical structures from the actual potential energy surface minimum, or due to a less accurate description of the intermolecular interactions in general, which leads to larger systematic errors, or both.

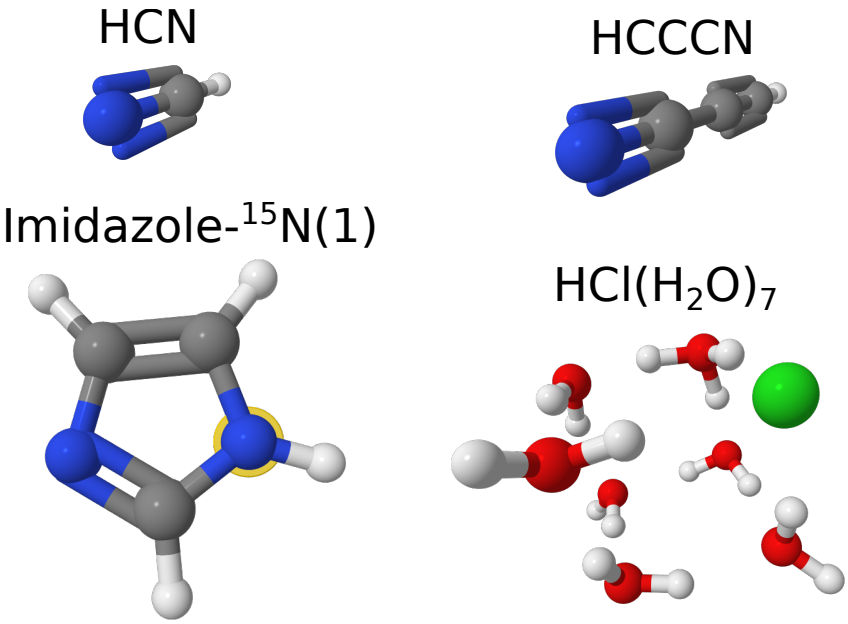

Figure 1. Examplary molecular systems to demonstrate the effect of scaling factors (see main text for details). The atomic color scheme is as follows: hydrogen—white; carbon—gray; nitrogen—blue; oxygen—red; and chlorine—green. The position of isotopic substitution in imidazole is shown with a yellow halo around the atom.

Table 2. A comparison of experimental and theoretical rotational constants for a few examples of molecular systems: HCN and HCCCN, an imidazole-^{15}N(1) isotopologue, and a $HCl(H_2O)_7$ cluster (see Figure 1). "B3LYP" denotes results at the B3LYP-D3(BJ)/def2-TZVP level of theory, and PBE0 denotes results at the PBE0-D3(BJ)/def2-TZVP level of theory. A comparison for all other molecular systems can be found in an Excel spreadsheet in the Supplementary Materials.

Molecular System	*A*/*B*/*C*	Rotational Constant Value [MHz]			
		Experimental	Theoretical		
			B3LYP	PBE0	
			$s = 1$	$s = 1$	$s = 0.988$
HCN [50]	*B*	44,316	44,941	44,969	44,415
HCCCN [51]	*B*	4549	4591	4593	4537
Imidazole-^{15}N(1) [48]	*A*	9695	9756	9850	9729
	B	9188	9218	9271	9157
	C	4716	4740	4776	4717
$HCl(H_2O)_7$ [33]	*A*	914	935	947	935
	B	737	739	750	740
	C	689	709	720	711

Table 3. Relative root mean square deviation (rRMSD, Equation (5)) and mean absolute deviation (MAD, Equation (8)) values for rotational constants from three illustrative test sets of molecular systems using the PBE0-D3(BJ)/def2-TZVP level of theory. The optimal scaling factor for this method ($s_{opt} = 0.988$) is taken from Table 1.

Dataset	rRMSD(s) × 100%		MAD(s) [MHz]	
	$s = 1$	$s = 0.988$	$s = 1$	$s = 0.988$
Linear molecules	1.0	0.3	33	16
Isotopologues	1.4	0.4	110	26
$HCl(H_2O)_n$	7.9	6.8	132	115

5. Conclusions

In this work, we introduced the concept of scaling factors for rotational constants. Applying a single tabulated scaling factor for all rotational constants was effectively equivalent to scaling the molecular size to account for systematic errors in the equilibrium structure due to the quantum–chemical approximation and for absent anharmonic effects. Sets of scaling factors for ten different DFT approximations, namely DF-Dn/def2-mVP (DF = B3LYP, PBE0; $n = 3(BJ), 4$; m = S, TZ) and PBEh-3c and r^{2}SCAN-3c, were produced from the database of 174 non-linear molecules. The applicability of these scaling factors was illustrated for the PBE0-D3(BJ)/def2-TZVP level of theory in the case of linear molecules, isotopologues, and non-covalently bonded systems. Thus, the application of such scaling factors can be recommended for the more accurate identification of species in rotational spectra and to support the assignment of specific molecular species in complicated broadband rotational spectra.

Supplementary Materials: The following supporting information can be downloaded at https://www.mdpi.com/article/10.3390/molecules29245874/s1.

Author Contributions: Conceptualization, D.S.T. and M.S.; methodology, D.S.T.; validation, D.S.T.; formal analysis, D.S.T., C.J.S., W.S., F.X., M.K., E.G., J.L., F.B., H.S. and C.M.T.; investigation, D.S.T., C.J.S., W.S., F.X., M.K., E.G., J.L., F.B., H.S. and C.M.T.; resources, M.S.; data curation, M.S.; writing—original draft preparation, D.S.T.; writing—review and editing, M.S.; supervision, M.S.; project administration, M.S.; funding acquisition, M.S. All authors have read and agreed to the published version of the manuscript.

Funding: C.J.S. acknowledges the Charles Hamilton Houston Internship Program at Amherst College that sponsored his internship at Deutsches Elektronen-Synchrotron DESY.

Institutional Review Board Statement: Not applicable

Informed Consent Statement: Not applicable

Data Availability Statement: The Excel sheet containing the data and computations for obtaining the scaling factors is provided in the Supplementary Materials.

Acknowledgments: All authors acknowledge DESY (Hamburg, Germany), a member of the Helmholtz Association HGF. In particular, D.S.T.'s calculations were enabled through the Maxwell computational resources operated at DESY.

Conflicts of Interest: The authors declare no conflicts of interest.

Abbreviations

The following abbreviations are used in this manuscript:

MW	microwave
MMW	millimeter wave
THZ	terahertz
QC	quantum–chemical
DFT	density functional theory
rRMSD	relative root mean square deviation
MAD	mean absolute deviation

References

1. Morino, Y.; Hirota, E. Microwave Spectroscopy. *Annu. Rev. Phys. Chem.* **1969**, *20*, 139–166. [CrossRef]
2. Park, G.B.; Field, R.W. Perspective: The first ten years of broadband chirped pulse Fourier transform microwave spectroscopy. *J. Chem. Phys.* **2016**, *144*, 200901. [CrossRef] [PubMed]
3. Prozument, K.; Barratt Park, G.; Shaver, R.G.; Vasiliou, A.K.; Oldham, J.M.; David, D.E.; Muenter, J.S.; Stanton, J.F.; Suits, A.G.; Barney Ellison, G.; et al. Chirped-pulse millimeter-wave spectroscopy for dynamics and kinetics studies of pyrolysis reactions. *Phys. Chem. Chem. Phys.* **2014**, *16*, 15739–15751. [CrossRef] [PubMed]
4. Cuisset, A.; Hindle, F.; Mouret, G.; Bocquet, R.; Bruckhuisen, J.; Decker, J.; Pienkina, A.; Bray, C.; Fertein, E.; Boudon, V. Terahertz Rotational Spectroscopy of Greenhouse Gases Using Long Interaction Path-Lengths. *Appl. Sci.* **2021**, *11*, 1229. [CrossRef]
5. Swearer, D.F.; Gottheim, S.; Simmons, J.G.; Phillips, D.J.; Kale, M.J.; McClain, M.J.; Christopher, P.; Halas, N.J.; Everitt, H.O. Monitoring Chemical Reactions with Terahertz Rotational Spectroscopy. *ACS Photonics* **2018**, *5*, 3097–3106. [CrossRef]
6. Giesen, T.; Brünken, S.; Caris, M.; Neubauer-Guenther, P.; Fuchs, U.; Lewen, F. Terahertz Rotational Spectroscopy. *Proc. Int. Astron. Union* **2005**, *231*, 87–96. [CrossRef]
7. Pinacho, P.; Quesada-Moreno, M.M.; Schnell, M. Conformations of borneol and isoborneol in the gas phase: Their monomers and microsolvation clusters. *J. Chem. Phys.* **2023**, *159*, 194305. [CrossRef]
8. Loru, D.; Cabezas, C.; Cernicharo, J.; Schnell, M.; Steber, A.L. Detection of ethynylbenzene in TMC-1 and the interstellar search for 1,2-diethynylbenzene. *A & A* **2023**, *677*, A166. [CrossRef]
9. Xie, F.; Sun, W.; Hartwig, B.; Obenchain, D.A.; Schnell, M. Hydrogen-Atom Tunneling in a Homochiral Environment. *Angew. Chem. Int. Ed.* **2023**, *62*, e202308273. [CrossRef] [PubMed]
10. Loru, D.; Steber, A.L.; Pérez, C.; Obenchain, D.A.; Temelso, B.; López, J.C.; Schnell, M. Quantum Tunneling Facilitates Water Motion across the Surface of Phenanthrene. *J. Am. Chem. Soc.* **2023**, *145*, 17201–17210. [CrossRef] [PubMed]
11. Li, W.; Tikhonov, D.S.; Schnell, M. Double Proton Transfer Across a Table: The Formic Acid Dimer–Fluorobenzene Complex. *Angew. Chem. Int. Ed.* **2021**, *60*, 25674–25679. [CrossRef] [PubMed]
12. Nguyen, H.V.L.; Caminati, W.; Grabow, J.U. The LAM of the Rings: Large Amplitude Motions in Aromatic Molecules Studied by Microwave Spectroscopy. *Molecules* **2022**, *27*, 3948. [CrossRef]
13. Carlotti, M.; Trombetti, A.; Velino, B.; Vrbancich, J. The rotation-inversion spectrum of 15NH3. *J. Mol. Spectrosc.* **1980**, *83*, 401–407. [CrossRef]
14. Krin, A.; Quesada Moreno, M.M.; Pérez, C.; Schnell, M. A Scent of Peppermint—A Microwave Spectroscopy Analysis on the Composition of Peppermint Oil. *Symmetry* **2022**, *14*, 1262. [CrossRef]
15. Sun, W.; Pinacho, P.; Obenchain, D.A.; Schnell, M. Gas-Phase Characterization of Adipic Acid, 6-Hydroxycaproic Acid, and Their Thermal Decomposition Products by Rotational Spectroscopy. *J. Phys. Chem. Lett.* **2024**, *15*, 817–825. [CrossRef] [PubMed]
16. Tretyakov, M. Spectroscopy underlying microwave remote sensing of atmospheric water vapor. *J. Mol. Spectrosc.* **2016**, *328*, 7–26. [CrossRef]
17. Muhleman, D.O.; Clancy, R.T. Microwave spectroscopy of the Mars atmosphere. *Appl. Opt.* **1995**, *34*, 6067–6080. [CrossRef]

18. Guélin, M.; Cernicharo, J. Organic Molecules in Interstellar Space: Latest Advances. *Front. Astron. Space Sci.* **2022**, *9*, 787567. [CrossRef]
19. Gordy, W.; Cook, R. *Microwave Molecular Spectra*, 3rd ed.; Wiley: New York, NY, USA, 1984.
20. Atkins, P.; Friedman, R. *Molecular Quantum Mechanics*; OUP: Oxford, UK, 2011.
21. Cristina Puzzarini, J.F.S.; Gauss, J. Quantum-chemical calculation of spectroscopic parameters for rotational spectroscopy. *Int. Rev. Phys. Chem.* **2010**, *29*, 273–367. [CrossRef]
22. Gottschalk, H.C.; Poblotzki, A.; Fatima, M.; Obenchain, D.A.; Pérez, C.; Antony, J.; Auer, A.A.; Baptista, L.; Benoit, D.M.; Bistoni, G.; et al. The first microsolvation step for furans: New experiments and benchmarking strategies. *J. Chem. Phys.* **2020**, *152*, 164303. [CrossRef] [PubMed]
23. Tikhonov, D.S.; Vishnevskiy, Y.V. Describing nuclear quantum effects in vibrational properties using molecular dynamics with Wigner sampling. *Phys. Chem. Chem. Phys.* **2023**, *25*, 18406–18423. [CrossRef] [PubMed]
24. Mata, R.A.; Suhm, M.A. Benchmarking Quantum Chemical Methods: Are We Heading in the Right Direction? *Angew. Chem. Int. Ed.* **2017**, *56*, 11011–11018. [CrossRef]
25. Pulay, P.; Fogarasi, G.; Pongor, G.; Boggs, J.E.; Vargha, A. Combination of theoretical ab initio and experimental information to obtain reliable harmonic force constants. Scaled quantum mechanical (QM) force fields for glyoxal, acrolein, butadiene, formaldehyde, and ethylene. *J. Am. Chem. Soc.* **1983**, *105*, 7037–7047. [CrossRef]
26. Irikura, K.K.; Johnson, R.D.; Kacker, R.N. Uncertainties in Scaling Factors for ab Initio Vibrational Frequencies. *J. Phys. Chem. A* **2005**, *109*, 8430–8437. [CrossRef] [PubMed]
27. Kesharwani, M.K.; Brauer, B.; Martin, J.M.L. Frequency and Zero-Point Vibrational Energy Scale Factors for Double-Hybrid Density Functionals (and Other Selected Methods): Can Anharmonic Force Fields Be Avoided? *J. Phys. Chem. A* **2015**, *119*, 1701–1714. [CrossRef] [PubMed]
28. Alecu, I.M.; Zheng, J.; Zhao, Y.; Truhlar, D.G. Computational Thermochemistry: Scale Factor Databases and Scale Factors for Vibrational Frequencies Obtained from Electronic Model Chemistries. *J. Chem. Theory Comput.* **2010**, *6*, 2872–2887. [CrossRef] [PubMed]
29. Laury, M.L.; Carlson, M.J.; Wilson, A.K. Vibrational frequency scale factors for density functional theory and the polarization consistent basis sets. *J. Comput. Chem.* **2012**, *33*, 2380–2387. [CrossRef] [PubMed]
30. Merrick, J.P.; Moran, D.; Radom, L. An Evaluation of Harmonic Vibrational Frequency Scale Factors. *J. Phys. Chem. A* **2007**, *111*, 11683–11700. [CrossRef] [PubMed]
31. Pople, J.A.; Scott, A.P.; Wong, M.W.; Radom, L. Scaling Factors for Obtaining Fundamental Vibrational Frequencies and Zero-Point Energies from HF/6–31G* and MP2/6–31G* Harmonic Frequencies. *Isr. J. Chem.* **1993**, *33*, 345–350. [CrossRef]
32. Khaikin, L.S.; Grikina, O.E.; Vogt, N.; Stepanov, N.F. Interpreting the vibrational spectra of uracil molecules and their deuterated isotopomers using a scaled quantum-chemical quadratic force field. *Russ. J. Phys. Chem. A* **2012**, *86*, 1855–1861. [CrossRef]
33. Xie, F.; Tikhonov, D.S.; Schnell, M. Electric nuclear quadrupole coupling reveals dissociation of HCl with a few water molecules. *Science* **2024**, *384*, 1435–1440. [CrossRef]
34. Tikhonov, D.S.; Gordiy, I.; Iakovlev, D.A.; Gorislav, A.A.; Kalinin, M.A.; Nikolenko, S.A.; Malaskeevich, K.M.; Yureva, K.; Matsokin, N.A.; Schnell, M. Harmonic scale factors of fundamental transitions for dispersion-corrected quantum chemical methods. *ChemPhysChem* **2024**, *25*, e202400547. [CrossRef]
35. Neese, F.; Wennmohs, F.; Becker, U.; Riplinger, C. The ORCA quantum chemistry program package. *J. Chem. Phys.* **2020**, *152*, 224108. [CrossRef]
36. Neese, F. Software update: The ORCA program system—Version 5.0. *WIREs Comput. Mol. Sci.* **2022**, *12*, e1606. [CrossRef]
37. Becke, A.D. Density-functional thermochemistry. III. The role of exact exchange. *J. Chem. Phys.* **1993**, *98*, 5648–5652. [CrossRef]
38. Becke, A.D. Density-functional exchange-energy approximation with correct asymptotic behavior. *Phys. Rev. A* **1988**, *38*, 3098–3100. [CrossRef]
39. Lee, C.; Yang, W.; Parr, R.G. Development of the Colle-Salvetti correlation-energy formula into a functional of the electron density. *Phys. Rev. B* **1988**, *37*, 785–789. [CrossRef]
40. Adamo, C.; Barone, V. Toward reliable density functional methods without adjustable parameters: The PBE0 model. *J. Chem. Phys.* **1999**, *110*, 6158–6170. [CrossRef]
41. Weigend, F.; Ahlrichs, R. Balanced basis sets of split valence, triple zeta valence and quadruple zeta valence quality for H to Rn: Design and assessment of accuracy. *Phys. Chem. Chem. Phys.* **2005**, *7*, 3297–3305. [CrossRef] [PubMed]
42. Grimme, S.; Ehrlich, S.; Goerigk, L. Effect of the damping function in dispersion corrected density functional theory. *J. Comput. Chem.* **2011**, *32*, 1456–1465. [CrossRef] [PubMed]
43. Caldeweyher, E.; Ehlert, S.; Hansen, A.; Neugebauer, H.; Spicher, S.; Bannwarth, C.; Grimme, S. A generally applicable atomic-charge dependent London dispersion correction. *J. Chem. Phys.* **2019**, *150*, 154122. [CrossRef] [PubMed]
44. Grimme, S.; Brandenburg, J.G.; Bannwarth, C.; Hansen, A. Consistent structures and interactions by density functional theory with small atomic orbital basis sets. *J. Chem. Phys.* **2015**, *143*, 054107. [CrossRef]
45. Grimme, S.; Hansen, A.; Ehlert, S.; Mewes, J.M. r2SCAN-3c: A "Swiss army knife" composite electronic-structure method. *J. Chem. Phys.* **2021**, *154*, 064103. [CrossRef] [PubMed]

46. Fokin, A.A.; Zhuk, T.S.; Blomeyer, S.; Pérez, C.; Chernish, L.V.; Pashenko, A.E.; Antony, J.; Vishnevskiy, Y.V.; Berger, R.J.F.; Grimme, S.; et al. Intramolecular London Dispersion Interaction Effects on Gas-Phase and Solid-State Structures of Diamondoid Dimers. *J. Am. Chem. Soc.* **2017**, *139*, 16696–16707. [CrossRef] [PubMed]
47. Vishnevskiy, Y.V. UNEX Version 1.6. Available online: https://unex.vishnevskiy.group (accessed on 13 October 2023).
48. Arenas, B.E.; Batra, G.; Steber, A.L.; Bizzocchi, L.; Pietropolli Charmet, A.; Giuliano, B.M.; Caselli, P.; Harris, B.J.; Pate, B.H.; Guillemin, J.C.; et al. Rotational spectroscopy of imidazole: Accurate spectroscopic information for three vibrationally excited states and the heavy-atom isotopologues up to 295 GHz. *J. Mol. Spectrosc.* **2021**, *378*, 111452. [CrossRef]
49. Kisiel, Z.; Białkowska-Jaworska, E.; Pszczółkowski, L.; Milet, A.; Struniewicz, C.; Moszynski, R.; Sadlej, J. Structure and properties of the weakly bound trimer $(H_2O)_2HCl$ observed by rotational spectroscopy. *J. Chem. Phys.* **2000**, *112*, 5767–5776. [CrossRef]
50. Winnewisser, G.; Maki, A.G.; Johnson, D.R. Rotational constants for HCN and DCN. *J. Mol. Spectrosc.* **1971**, *39*, 149–158. [CrossRef]
51. Creswell, R.; Winnewisser, G.; Gerry, M.C.L. Rotational spectra of the ^{13}C and ^{15}N isotopic species of cyanoacetylene. *J. Mol. Spectrosc.* **1977**, *65*, 420–429. [CrossRef]